

A 2^{7-3} fractional factorial optimization of polybenzimidazole based membrane electrode assemblies for H_2/O_2 fuel cells

R. Kannan · Md. N. Islam · D. Rathod · M. Vijay ·
U. K. Kharul · P. C. Ghosh · K. Vijayamohanana

Received: 23 August 2007 / Revised: 8 December 2007 / Accepted: 19 December 2007 / Published online: 4 January 2008
© Springer Science+Business Media B.V. 2008

Abstract We describe the usefulness of a statistical fractional factorial design to obtain consistent and reproducible behavior of a membrane-electrode-assembly (MEA) based on a phosphoric acid (PA) doped polybenzimidazole (PBI) membrane, which allows a H_2/O_2 fuel cell to operate above 150 °C. Different parameters involved during the MEA fabrication including the catalyst loading, amount of binder, processing conditions like temperature and compaction load and also the amount of carbon in the gas diffusion layers (GDL) have been systematically varied according to a 2^{7-3} fractional factorial design and the data thus obtained have been analyzed using Yates's algorithm. The mean effects estimated in this way suggest the crucial role played by carbon loading in the gas diffusion layer, hot compaction temperature and the binder to catalyst ratio in the catalyst layer for enabling continuous performance. These statistically designed electrodes provide a maximum current density and power density of $1,800 \text{ mA cm}^{-2}$ and 280 mW cm^{-2} , respectively, at 160 °C using hydrogen and oxygen under ambient pressure.

Keywords PEMFC · Fractional factorial optimization · MEA · PBI · Carbon loading

1 Introduction

Polymer electrolyte membrane fuel cells (PEMFCs) have attracted much attention because of their promise as clean

energy conversion devices for both mobile and stationary applications [1, 2]. This is mainly because of their high power density facilitating higher energy conversion efficiency especially due to low weight and volume, in addition to benefits associated with the ease of fabrication and insignificant emission level. However, commercial realization of PEMFCs for practical applications is still limited by several material and process related issues [1]. For example, the widely used perfluorosulphonic acid polymer electrolyte, (Nafion[®]) depends critically on water for its ionic conduction, thus restricting its operating temperature to less than 100 °C. Water management at these temperatures is difficult as it increases the system complexity and flooding of cathodes by product water is one of the common problems associated with low temperature fuel cells [3–8]. Further, low operating temperature necessitates the use of ultra pure H_2 as the fuel and consequently the fuel cells will become more expensive. In the case of using reformed H_2 , the poisoning of anode electrocatalyst by CO is another important issue that remains unsolved [9–19]. To alleviate these problems, it is interesting to work at temperatures higher than 100 °C. Such elevated temperature operation of PEMFC entails many advantages for both automotive and stationary applications like higher rates, more efficient water and thermal management, and finally improved CO tolerance by the electrocatalysts. However, the absence of a suitable thermally stable membrane with good proton conductivity obviates further development [20].

Extensive efforts have been expended recently to develop membranes that can operate at temperatures more than 100 °C and among various alternatives, phosphoric acid (PA) doped polybenzimidazole (PBI) is a potential candidate with low cost and high performance [20–45]. One of the important benefits associated with this membrane

R. Kannan · Md. N. Islam · D. Rathod · M. Vijay ·
U. K. Kharul · P. C. Ghosh · K. Vijayamohanana (✉)
National Chemical Laboratory, Dr. Homi Bhabha Road,
Pune 411008, India
e-mail: vk.pillai@ncl.res.in

includes the increased tolerance for CO poisoning at higher operating temperatures ($>150\text{ }^{\circ}\text{C}$). For example, a tolerance level of 3% CO in hydrogen is observed at $200\text{ }^{\circ}\text{C}$ at current densities up to 0.8 A cm^{-2} compared to only 100 ppm level of CO at $80\text{ }^{\circ}\text{C}$ as reported by Li et al. [11]. More importantly, the protonic conduction is independent of membrane water content (or to the humidification level of the inlet gases) and their electro-osmotic drag coefficient is essentially zero, thus greatly simplifying the parasitic load of the system. This is especially significant for H_2/O_2 fuel cells operating with reformed hydrogen as the fuel [19]. Higher operating temperatures also increase the kinetics of the oxygen reduction reaction (ORR), which is, one of the limiting factors of PEM fuel cell performance [46–48].

In recent years, several groups have devoted attention to PBI membranes and almost all the efforts were focused on either improving the membrane behavior along with enhanced ionic conductivity or increasing their mechanical and chemical stability [20–45, 49–53]. However, few efforts have focused on the fabrication of the membrane-electrode-assembly (MEA), despite its importance in developing stacks. This is in direct contrast to the case of Nafion membrane based fuel cells, where the impact of each parameter has been well studied during the last two decades [54, 55]. For example, the effect of catalyst ink preparation method has been studied by Lobato et al. using acetone and dimethylacetamide as solvents [56]. A detailed study on the impact of PBI binder in the catalyst layer of anode and cathode has been carried out along with different platinum to carbon ratio by Seland et al. [57]. Nevertheless, the role of other parameters like compaction temperature, pressure and amount of carbon in the gas diffusion layer (GDL) has not been studied systematically. This is specially significant since a minor variation in one of these factors can cause a dramatic change in MEA performance and hence statistical methods are essential to ensure reproducible behavior arising out of multiple interactions of these process variables [58].

Factorial experiments are one of the most efficient designs when multiple parameters interact significantly among themselves and when they have a complementary impact on each other [59–63]. Further, factorial experiments can point the way to the choice of conditions outside those originally selected by means of which a greater response of the required parameter can be achieved using the “method of steepest ascent”. However, one big drawback with factorial design is that the total number of experiments goes up sharply as the number of factors, thus requiring too much time and resources for optimization. The use of fractional factorial experiments can greatly reduce this number of experiments facilitating a quicker realization through the path of steepest ascent [61–63]. The principle of fractional factorial experiment is that when the

higher order effects of two or more combination of experiments are the same, they cannot be distinguished from one another, and hence they can be aliased, thus reducing the total number of experiments.

In this work we describe a 2^{7-3} fractional factorial design of a PBI based MEA fabrication by analyzing the effect of different parameters such as compaction temperature, pressure, amount of carbon, catalyst and binder in the electrode. The mean effect of each of these parameters as well as their mutual interactions have been analyzed with rigorous error variation (analysis of variance) through Yate’s algorithm and the final optimized design has been accomplished based on the path of steepest ascent. Polarization measurements carried out using these optimally designed MEAs deliver consistently a current density and power density of $1,800\text{ mA cm}^{-2}$ and 280 mW cm^{-2} , respectively, at $160\text{ }^{\circ}\text{C}$ under ambient pressure using pure H_2 and O_2 .

2 Experimental

2.1 Membrane fabrication

The PBI was synthesized from diaminobenzidine (DAB) and isophthalic acid (IPA, AR Grade) using polyphosphoric acid as a solvent at $200\text{ }^{\circ}\text{C}$ for 20 h as reported by Iwakura et al. [64]. The inherent viscosity of the polymer was 1.2 dL g^{-1} in conc. H_2SO_4 (concentration: 0.2 g dL^{-1}). The dense membrane was prepared by the solution casting method. Typically a 3% PBI solution in *N,N*-dimethylacetamide (DMAc) was heated to $80\text{--}90\text{ }^{\circ}\text{C}$ and kept for 16 h under dry conditions. The film was subsequently peeled off and treated with water at $60\text{ }^{\circ}\text{C}$ for a week and was then dried under vacuum at $100\text{ }^{\circ}\text{C}$ for 2 days before doping. The membrane was dipped in 88% H_3PO_4 (PA) solution for 72 h and then vacuum dried at $100\text{ }^{\circ}\text{C}$ for 2 days. The PA uptake was estimated to be ~ 13 moles per repeating unit, gravimetrically.

2.2 Fractional factorial design

Seven parameters selected for the fractional factorial design based on the preliminary screening experiments along with their normal range are given in Table 1. These were selected based on literature reports for Nafion based membranes and on previous experience with PBI based membranes in our laboratory. Since 128 experiments were required for completing a 2^7 factorial optimization study, we decided to carry out a 2^{7-3} fractional factorial optimization design, in order to avoid unnecessary waste of time and resources. The design of 16 experiments with the

Table 1 Parameters considered for the 2^{7-3} fractional factorial optimization along with their range and code

| Parameter code | Parameter | Levels | |
|----------------|---|--------------------------|---------------------------|
| | | High | Low |
| A | Amount of binder in the catalyst layer | 1 mg cm ⁻² | 0.2 mg cm ⁻² |
| B | Electrocatalyst loading | 1 mg cm ⁻² | 0.1 mg cm ⁻² |
| C | Amount of carbon in the gas diffusion layer | 4.5 mg cm ⁻² | 2 mg cm ⁻² |
| D | Hot compaction time | 10 min | 1 min |
| E | Compaction temperature | 150 °C | 100 °C |
| F | Hot compaction load | 0.2 ton cm ⁻² | 0.04 ton cm ⁻² |
| G | Amount of PTFE in the gas diffusion layer | 1 mg cm ⁻² | 0.1 mg cm ⁻² |

combination of different parameters from A to G for a 2^{7-3} fractional factorial algorithm is given in Table 2. First column of Table 2 gives the experiment code while the last column suggests the corresponding treatment combination of that experiment.

2.3 Fabrication of MEA

Two carbon cloths of size 5×5 cm² were made hydrophobic by imbibing them in 15% Teflon (PTFE) emulsion (Fuel cell stores Inc), followed by air drying for 30 min. They were further heat treated at 350 °C for 5 h to adhere the PTFE with carbon cloth. Carbon ink was made by combining appropriate amount of Vulcan XC-72 carbon (Cabot Corporation) with PTFE emulsion in cyclohexane after ultrasonically mixing for 30 min. This ink was brushed on the carbon cloths till it reached the desired loading

levels. The loading levels were double in the membrane facing side of the carbon cloth. These carbon cloths were cold pressed at 0.5 ton for 1 min and then kept in a furnace at 350 °C for 30 min.

Catalyst ink was prepared by adding 20% Pt/C and 1% PBI solution in DMAc. This mixture was ultrasonicated for 30 min and the resulting ink was brushed on the surface of the GDL in a hot plate until the desired loading was reached. On top of the catalyst layer a thin layer of PBI solution was given and the resulting electrodes were dried and hot pressed uni-axially with the PA doped PBI membrane. This MEA was kept in a desiccator for 1 day in order for the catalyst layer to become saturated with the excess PA present in the membrane. SEM images were taken for four different combinations of carbon and PTFE and for the optimized design (Leica Stereoscan 440 model EDAX system). All the GDLs prepared were of four combinations; indicated as GDL 1–4. GDL 1: 2 mg cm⁻²

Table 2 Various treatment combinations corresponding to the fractional factorial design of 2^{7-3} experiments

| Exp code | A (mg cm ⁻²) | B (mg cm ⁻²) | C (mg cm ⁻²) | D (min) | E (°C) | F (ton cm ⁻²) | G (mg cm ⁻²) | Treatment combination |
|----------|--------------------------|--------------------------|--------------------------|---------|--------|---------------------------|--------------------------|-----------------------|
| F1 | 0.2 | 0.1 | 2.0 | 1 | 100 | 0.04 | 0.1 | 1 |
| F2 | 1 | 0.1 | 2.0 | 1 | 150 | 0.2 | 1 | aefg |
| F3 | 0.2 | 1 | 2.0 | 1 | 150 | 0.2 | 0.1 | bef |
| F4 | 1 | 1 | 2.0 | 1 | 100 | 0.04 | 1 | abg |
| F5 | 0.2 | 0.1 | 4.5 | 1 | 150 | 0.04 | 1 | ceg |
| F6 | 1 | 0.1 | 4.5 | 1 | 100 | 0.2 | 0.1 | acf |
| F7 | 0.2 | 1 | 4.5 | 1 | 100 | 0.2 | 1 | bcfg |
| F8 | 1 | 1 | 4.5 | 1 | 150 | 0.04 | 0.1 | abce |
| F9 | 0.2 | 0.1 | 2.0 | 10 | 100 | 0.2 | 0.1 | df |
| F10 | 1 | 0.1 | 2.0 | 10 | 150 | 0.04 | 0.1 | ade |
| F11 | 0.2 | 1 | 2.0 | 10 | 150 | 0.04 | 1 | bdeg |
| F12 | 1 | 1 | 2.0 | 10 | 100 | 0.2 | 0.1 | abdf |
| F13 | 0.2 | 0.1 | 4.5 | 10 | 150 | 0.2 | 0.1 | cdef |
| F14 | 1 | 0.1 | 4.5 | 10 | 100 | 0.2 | 0.1 | acdg |
| F15 | 0.2 | 1 | 4.5 | 10 | 100 | 0.04 | 0.1 | bcd |
| F16 | 1 | 1 | 4.5 | 10 | 150 | 0.2 | 1 | abcdefg |

carbon and 0.1 mg cm^{-2} PTFE, GDL 2: 2 mg cm^{-2} carbon and 1 mg cm^{-2} PTFE, GDL 3: 5 mg cm^{-2} carbon and 0.1 mg cm^{-2} PTFE, GDL 4: 5 mg cm^{-2} carbon and 1 mg cm^{-2} PTFE. The combination of GDL 5 was that of the optimized design i.e. F18.

2.4 Fuel cell testing

All the MEAs were tested on an Arbin fuel cell test station (Model: Arbin-001 MITS Pro-FCTS 5.0-FCTS) under non-humidified conditions. Prior to the testing, the MEA was conditioned by monitoring the open circuit potential (OCV) for 30 min to ensure its stability at constant temperature ($160 \text{ }^\circ\text{C}$) and subsequently conditioned at 0.2 V for 30 min after which polarization measurements were carried out. A pin type flow field was used and H_2 and O_2 flow rates were maintained constant at 1 slpm. The cells were operated at $160 \text{ }^\circ\text{C}$ through a pair of external electrical heating elements.

3 Results and discussion

Figure 1 shows the polarization plot obtained for all the MEAs as per the 2^{7-3} design. A dramatic change in performance from 4 to $1,100 \text{ mA cm}^{-2}$ due to the variations in the fabrication conditions can be observed. The maximum current density obtained in each experiment is considered as the main response for calculating the mean effects as given in the third column of Table 3. From Fig. 1 and Table 3, it is clear that F9 gives the maximum current density of $1,100 \text{ mA cm}^{-2}$ where the carbon loading is 2 mg cm^{-2} . Similarly, MEAs with less carbon loading (2 mg cm^{-2}) (Fig. 1a) give better performance compared to MEAs of higher carbon loading (4.5 mg cm^{-2}) (Fig. 1b) considering equal level of all other parameters. The maximum current density obtained with higher carbon loading

is 87 mA cm^{-2} , which is far less compared to that of MEAs with lower carbon loading. Even though other parameters in the fabrication are also varied during those experiments, a close inspection reveals the critical role of the amount of carbon in the diffusion layer than that of all other parameters. This may be due to the blocking of the gas transport by the excess carbon present in the GDL, hindering access to the catalyst layer at the electrode–electrolyte interface. This is further confirmed by the SEM images shown in Figs. 2 and 3. For example, it can be seen from Fig. 2 that in GDL 1 and 3 where the carbon loading is less, the morphology of bare carbon cloth is observable even after brushing carbon to prepare the gas diffusion layer, while in GDL 2 and 4, only a uniform and dense layer of carbon can be seen. Further, in Fig. 3, we can see the micro pores in GDL 1, but in GDL 2 and 4, they are hardly observed because of the higher carbon content, which reduces the porosity. However, these micro pores are not seen in GDL 3 even though the carbon loading is less. This can be attributed to the high content of PTFE that binds the carbon together leading to a layered sheet like structure with less pores. All these factors, contribute to the higher current density obtained with F9, where the GDL composition is that of GDL 1.

Another factor with a significant impact on the performance of the MEA is hot compaction temperature. The maximum current density values are obtained with lower hot compaction temperature perhaps due to the fact that pressing the membranes at higher temperature could cause the membrane to loose its mechanical stability concomitantly leading to the leaching out of additional PA from the membrane. This was further confirmed by separate experiments by hot pressing membranes at 100 and $150 \text{ }^\circ\text{C}$, respectively at a pressure of 3 tons for 5 min to show a corresponding weight loss of 8% and 13%. Hence, the high leaching of PA may be the primary reason behind the poor performance of MEAs with higher compaction temperatures. The remaining parameters also play crucial roles in

Fig. 1 Polarization plots obtained during the fractional factorial optimization experiments. (a) MEAs with lower carbon loading, (b) MEA with higher carbon loading. The cells were operated at $160 \text{ }^\circ\text{C}$ with Pure H_2 and O_2 as fuel and oxidant. The details of the experiment combinations from F1 to F16 are given in Table 2

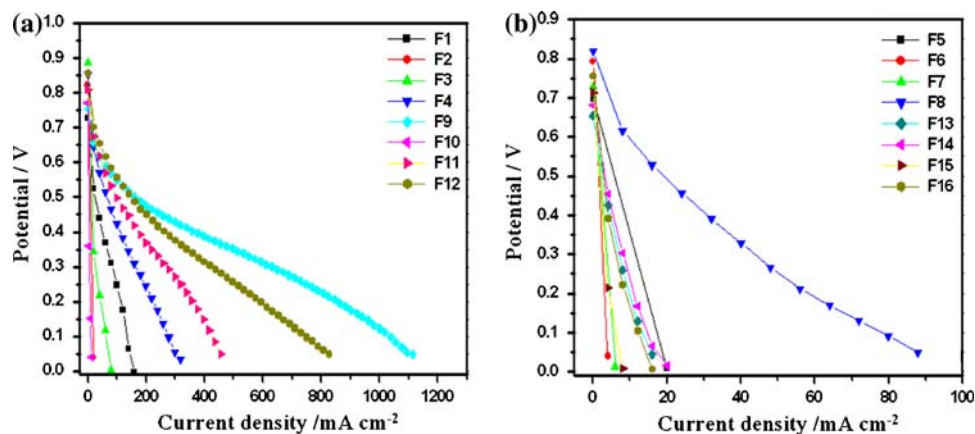
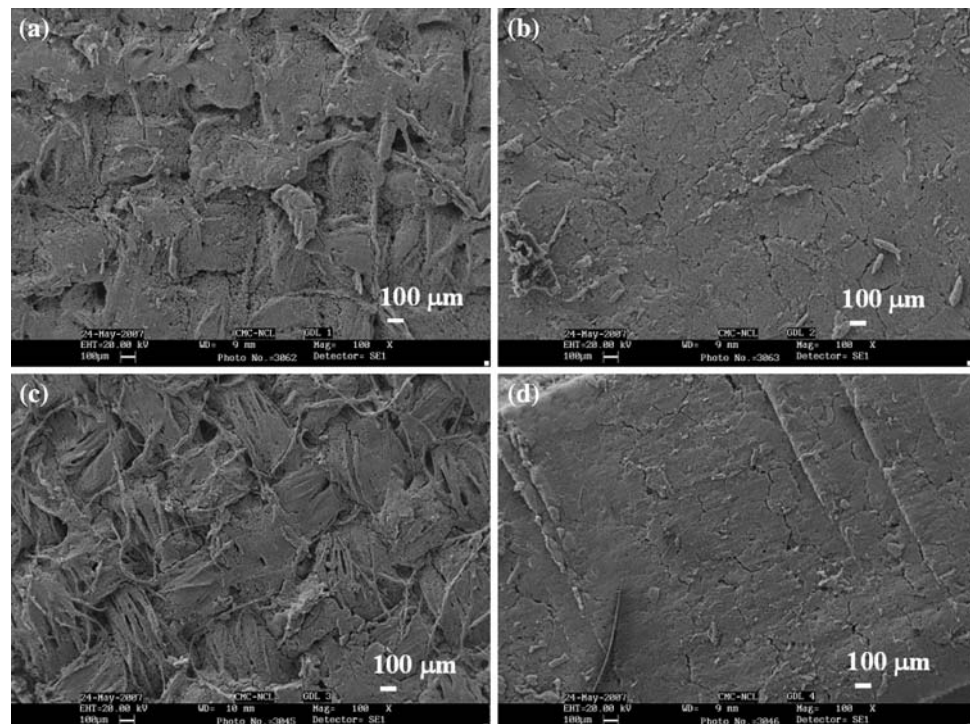


Table 3 Yate’s analysis on the current density values obtained for the treatment combinations from the 2⁷⁻³ experiments and the mean effect values along with the corresponding factor

| Exp code | Treatment | Response (CD/mA cm ⁻²) | Analysis | | | | Mean effect | Factor |
|----------|-----------|------------------------------------|----------|-------|--------|---------|-------------|------------|
| | | | I | II | III | IV | | |
| F1 | 1 | 160 | 180 | 577 | 707.7 | 3310.7 | 51.72969 | Mean total |
| F2 | aefg | 20 | 397 | 130.7 | 2603 | -599.3 | -9.364063 | A |
| F3 | bef | 80 | 23 | 2544 | 149.7 | 608.7 | 9.510938 | B |
| F4 | abg | 317 | 107.7 | 59 | -749 | 1878.7 | 29.35469 | AB |
| F5 | ceg | 19 | 1112 | 97 | 301.7 | -2931.3 | -45.80156 | C |
| F6 | acf | 4 | 1432 | 52.7 | 307 | 726.7 | 11.35469 | DG |
| F7 | bcfg | 20 | 36 | -760 | 459.7 | -465.3 | -7.270313 | FG |
| F8 | abce | 87.7 | 23 | 11 | 1419 | -1707.3 | -26.67656 | E |
| F9 | df | 1100 | -140 | 217 | -446.3 | 1895.3 | 29.61406 | D |
| F10 | ade | 12 | 237 | 84.7 | -2485 | -898.7 | -14.04219 | AD |
| F11 | bdeg | 552 | -15 | 320 | -44.3 | 5.3 | 0.082813 | BD |
| F12 | abdf | 880 | 67.7 | -13 | 771 | 959.3 | 14.98906 | F |
| F13 | cdef | 16 | -1088 | 377 | -132.3 | -2038.7 | -31.85469 | AG |
| F14 | acdg | 20 | 328 | 82.7 | -333 | 815.3 | 12.73906 | G |
| F15 | bcd | 8 | 4 | 1416 | -294.3 | -200.7 | -3.135938 | DFG |
| F16 | abcdefg | 15 | 7 | 3 | -1413 | -1118.7 | -17.47969 | DE |

Fig. 2 SEM images of (a) GDL 1, (b) GDL 2, (c) GDL 3, (d) GDL 4. GDL 1–4 are made with different carbon and binder ratio according to the factorial design and the details are given in experimental section

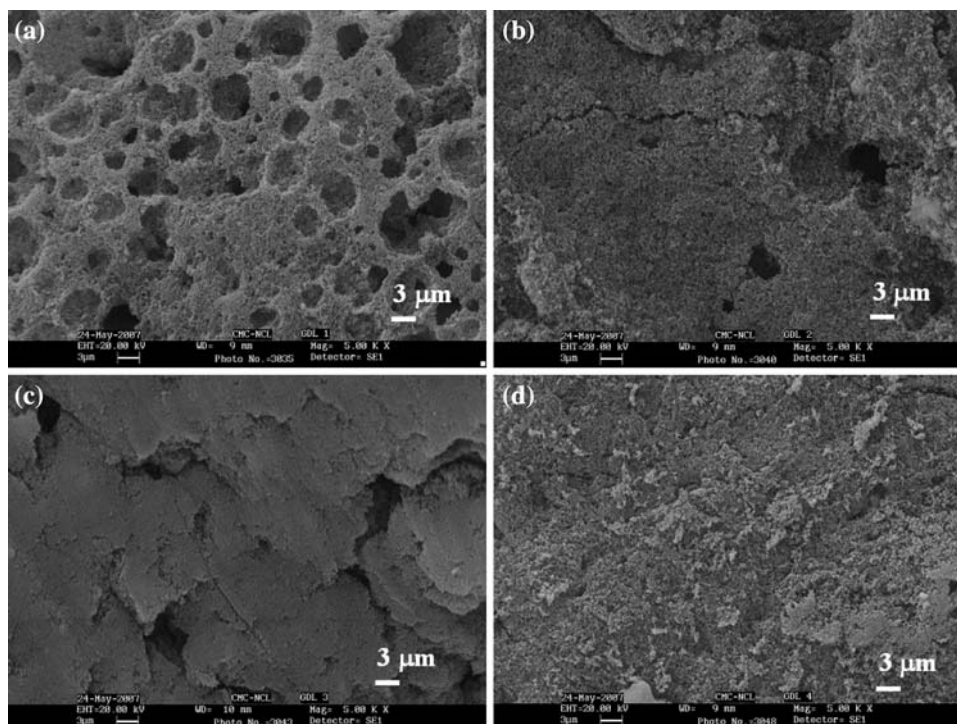


fuel cell performance, although their effects are not as apparent as that of carbon loading and hot compaction temperature. Since Yate’s algorithm helps to find the relative impact of each parameter quantitatively on the performances of MEAs in a systematic manner, all the mean effects estimated accordingly are shown in Table 3.

3.1 YATE’s analysis

Yates devised a simple technique for estimating the effects and determining the sums of squares in a 2^{k-p} fractional factorial design and Table 3 is built based on this strategy. Consider the column 3 (response) of Table 3. The treatment

Fig. 3 Magnified SEM images of (a) GDL 1, (b) GDL 2, (c) GDL 3, (d) GDL 4. GDL 1–4 are made with different carbon and binder ratio according to the factorial design and the details are given in experimental section



combinations are written down in standard order and this column contains the observations of each experiment. The first half of the analysis column (I) is obtained by adding the responses in adjacent pairs. The second half is obtained by changing the sign of the first entry in each of the pairs in the response column and adding the adjacent pairs. Column (II) is obtained from column (I) just as column (I) is obtained from the response column and in a similar fashion column (III) and (IV) also obtained from (II) and (III). In general for a 2^{k-p} design, $k-p$ times the analysis has to be carried out. The mean effect values are calculated from this column.

Each mean effect value in Table 3 has a sign signifying the need for either increasing (positive sign) or decreasing (negative sign) the particular parameter from the mid range to achieve the optimum as per the method of steepest ascent. For example, the amount of carbon in the gas diffusion layer has to be decreased from its midpoint (-45.8) while the amount of catalyst in the catalyst layer has to be

increased from its average (9.5), indicating the constructive impact of both these parameters on cell performance.

In order to optimize all the parameters and to follow the path of steepest ascent, the experimental variable with maximum mean effect has to be identified first and for our case this is the amount of carbon loading on the gas diffusion layer (-45.8). For further optimization it is feasible to consider a decrease in the carbon loading in 0.25 mg cm^{-2} steps from the average value (one-fifth of the range of carbon loadings). Hence, six further experiments were designed for locating the global maximum for the MEA fabrication and accordingly the required step change for all other parameters have also been calculated. This final design of six such experiments to accomplish the maximum performance of our PBI based MEA accordingly, is given in Table 4.

Figure 4 shows the polarization plot for MEAs specially designed as per the final optimization plan of F17 to F22 (Table 4). Interestingly, F18 gives the best performance of

Table 4 Design optimization based on 2^{7-3} fractional factorial experiments; step change for each parameter has been calculated by $(P/-45.8) \times Q$, where P is the mean effect of each parameter and Q is one sixth of its range

| Experiments | A (mg cm^{-2}) | B (mg cm^{-2}) | C (mg cm^{-2}) | D (min) | E ($^{\circ}\text{C}$) | F (ton cm^{-2}) | G (mg cm^{-2}) |
|-------------|---------------------------|---------------------------|---------------------------|---------|--------------------------|----------------------------|---------------------------|
| F17 | 0.6 | 0.55 | 3.25 | 5.5 | 125 | 0.12 | 0.55 |
| F18 | 0.567 | 0.587 | 3 | 6.66 | 119.18 | 0.13 | 0.6 |
| F19 | 0.534 | 0.624 | 2.75 | 7.82 | 113.34 | 0.14 | 0.65 |
| F20 | 0.501 | 0.661 | 2.5 | 8.98 | 107.5 | 0.151 | 0.7 |
| F21 | 0.468 | 0.698 | 2.25 | 10.14 | 101.66 | 0.162 | 0.75 |
| F22 | 0.435 | 0.735 | 2 | 11.3 | 95.82 | 0.172 | 0.8 |

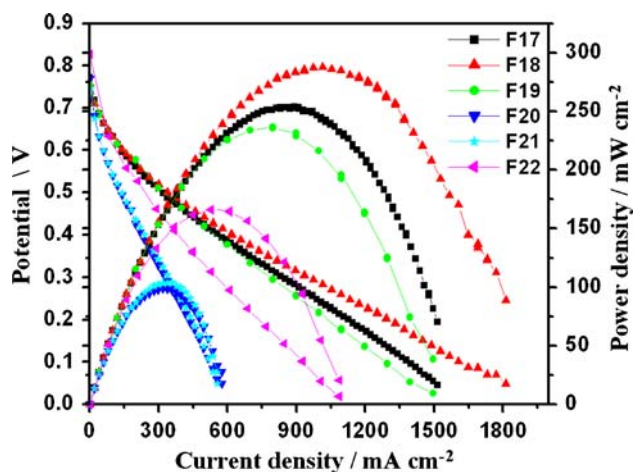
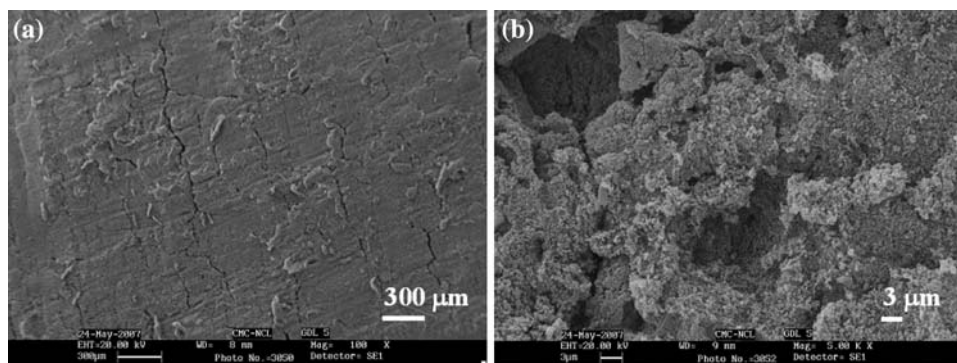


Fig. 4 Polarization plot of the design optimization experiments from F17 to F22. The details of the combinations are given in Table 4

1,800 mA cm⁻² as maximum current density, compared to all other treatment combinations although the preliminary design provides a maximum current density of only 1,100 mA cm⁻². The SEM image of the GDL of F18 (GDL 5) helps to rationalize this performance with the electrode morphology (Fig. 5) since the GDL 5 surface reveals much reduced pore size and density in comparison with GDL 1. This presumably helps to keep the catalyst layer intact on the side of the membrane, thus preventing the catalyst particles crossing the GDL. This, in turn, ensures maximum efficient utilization of the catalyst particles contributing to enhanced performance. However, the performance decreases further (F19 to F22) regardless of the small increment in F22 indicating the likelihood of a global maximum close to the combination represented by F18. From these results it can be surmised that a 1:1 catalyst to the binder ratio, hot compaction temperature of ~120 °C, and a hot pressing time of 6.66 min with a hot compaction load of 0.13 ton cm⁻² represent the best combination to obtain maximum performance of these PBI based MEAs at 160 °C. The reproducibility of performance has been confirmed by fabricating a total of five identical MEAs with the above optimum parameters and their estimated standard variation in performance is 4%.

Fig. 5 SEM images of the GDL of optimized design F18 at two different magnifications. The carbon and PTFE loadings are given in Table 4



Although fractional 2⁷⁻³ factorial experiments have been successful in locating the global maximum with the help of 16 experiments as per the design and six experiments for confirmation, there are some limitations. A countless number of factors can contribute to the performance of a fuel cell, while we have tested only a few. For example, the operating conditions and inlet gas flow rates can also alter the performance. This has not been considered in our study. Further, several membranes are being used for high temperature applications under the generic name of PBI and some properties might differ for each of them. Despite these limitations, the importance of this kind of fractional factorial study for MEA fabrication is reflected by the performance enhancement (about 160%), which undoubtedly suggests the usefulness of these techniques in fuel cell research.

4 Conclusions

We have used a 2⁷⁻³ fractional factorial optimization for the fabrication of PBI based fuel cells to accomplish a current density and power density of 1,800 mA cm⁻² and 280 mW cm⁻², respectively for a continuous operation at 160 °C. The impact of all key variables like the amount of carbon in the gas diffusion layer and the electrocatalyst loading have been quantitatively analyzed using their mean effect values and a judicious analysis of their interactions has led to a global optimum by design. The same statistical design could also be utilized for analyzing MEA life or membrane durability as output parameters and further experiments are in progress for understanding these effects with respect to the performance of our PBI based fuel cells.

Acknowledgments The authors are grateful to the Council of Science and Industrial Research, New Delhi, India, for funding through a NMITLI programme to carry out this work. RK thanks University Grants Commission for financial support. We also thank Dr. S. Sivaram, Director, National Chemical Laboratory, Pune and Prof. A.K. Shukla, Director, Central Electrochemical Research Institute, Karaikudi, for several valuable discussions.

Reference

1. Steel BCH, Heinze A (2001) *Nature* 414:345
2. Dresselhaus MS, Thomas IL (2001) *Nature* 414:332
3. Wilikinson DP, Voss HH, Prater K, (1994) *J Power Sources* 49:117
4. Mosdale R, Srinivasan S (1995) *Electrochim Acta* 40:413
5. Zawodzinski TA, Davey J, Valerio J, Gottesfeld S (1995) *Electrochim Acta* 40:297
6. van Nguyen T, Knobbe MW (2003) *J Power Sources* 114:70
7. van Bussel HPLH, Koene FGH, Mallant RKAM (1998) *J Power Sources* 71:218
8. Ren X, Henderson W, Gottesfeld S (1997) *J Electrochem Soc* 144:L267
9. Gottesfeld S, Pafford J (1988) *J Electrochem Soc* 135:2651
10. Springer TE, Rockward T, Zawodzinski TA, Gottesfeld S (2001) *J Electrochem Soc* 148:A11
11. Li Q, He R, Gao JA, Jensen JO, Bjerrum NJ (2003) *J Electrochem Soc* 150:A1599
12. Chu HS, Wang CP, Liao WC, Yan WM (2006) *J Power Sources* 159:1071
13. Wang C-P, Chu H-S (2006) *J Power Sources* 1059:1025
14. Bhatia KK, Wang C-Y (2004) *Electrochim Acta* 49:2333
15. Krishnan P, Park J-S, Kim C-S (2006) *J Power Sources* 159:817
16. Xu H, Song Y, Kunz HR, Fenton JM (2006) *J Power Sources* 159:979
17. Cheng X, Shi Z, Glass N, Zhang L, Zhang J, Song D, Liu Z-S, Wang H, Shen J (2007) *J Power Sources* 165:739
18. Uchida H, Izumi K, Watanabe M (2006) *J Phys Chem B* 110:21924
19. Holladay JD, Wainright JS, Jones EO, Gano SR (2004) *J Power Sources* 130:111
20. Li Q, He R, Jensen JO, Bjerrum NJ (2003) *Chem Mater* 15:4896
21. Gieselman MB, Reynolds JR (1993) *Macromolecules* 26:5633
22. Wainright JS, Wang J-T, Weng D, Savinell RF, Litt M (1995) *J Electrochem Soc* 142:L121
23. Staiti P, Lufrano F, Aricò AS, Passalacqua E, Antonucci V (2001) *J Memb Sci* 188:71
24. Fontanella JJ, Wintersgill MC, Wainright JS, Savinell RF, Litt M (1998) *Electrochim Acta* 43:1289
25. Kawahara M, Morita J, Rikukawa M, Sanui K, Ogata N (2000) *Electrochim Acta* 45:1395
26. Kerres JA (2001) *J Memb Sci* 185:3
27. Jalani NH, Ramani M, Ohlsson K, Buelte S, Pacifico G, Pollard R, Staudt R, Datta R (2006) *J Power Sources* 160:1096
28. Carollo A, Quartarone E, Tomasi C, Mustarelli P, Belotti F, Magistris A, Maestroni F, Parachini M, Garlaschelli L, Roghetti PP (2006) *J Power Sources* 160:175
29. Li Q, He R, Jensen JO, Bjerrum NJ (2004) *Fuel Cells* 4:147
30. He R, Li Q, Bach A, Jensen JO, Bjerrum NJ (2006) *J Memb Sci* 277:38
31. Wang J-T, Savinell RF, Wainright J, Litt M, Yu H (1996) *Electrochim Acta* 41:193
32. Kongstein OE, Berning T, Børresen B, Seland F, Tunold R (2007) *Energy* 32:418
33. Li Q, He R, Berg RW, Hjuler HA, Bjerrum NJ (2004) *Solid State Ionics* 168:177
34. Xiao G, Li Q, Hjuler HA, Berg RW, Bjerrum NJ (1995) *J Electrochem Soc* 142:2890
35. Xing B, Savadogo O (2000) *J New Mater Electrochem Syst* 3:345
36. Pu H, Meyer WH, Wegner G (2002) *J Polym Sci Part B Polym Phys* 40:663
37. Bouchet R, Siebert E (1999) *Solid State Ionics* 118:287
38. Ma Y-L, Wainright JS, Litt MH, Savinell RF (2004) *J Electrochem Soc* 151:A8
39. Li Q, Hjuler HA, Bjerrum NJ (2001) *J Appl Electrochem* 31:773
40. Lobato J, Canizares P, Rodrigo MA, Linares JJ, Manjavacas G (2006) *J Memb Sci* 280:351
41. Li Q, He R, Gao J-A, Jensen JO, Bjerrum NJ (2003) *J Electrochem Soc* 150:A1599
42. Weng D, Wainright JS, Landau U, Savinell RF (1996) *J Electrochem Soc* 143:1260
43. Xiao L, Zhang H, Jana T, Scanlon E, Chen R, Choe E-W, Ramanathan LS, Yu S, Benicewicz BC (2005) *Fuel Cells* 5:287
44. Saegusa Y, Horikiri M, Nakamura S (1997) *Macromol Chem Phys* 198:619
45. Chuang S-W, Hsu SL-C (2006) *J Polym Sci Part A Polym Chem* 44:4508
46. Zhang J, Sasaki K, Sutter E, Adzic RR (2007) *Science* 315:220
47. Stamenkovic VR, Fowler B, Mun BS, Wang G, Ross PN, Lucas CA, Markovic NM (2007) *Science* 315:493
48. Bashyam R, Zelanay P (2006) *Nature* 443:63
49. Staiti P, Minutoli M (2001) *J Power Sources* 94:9
50. Lobato J, Cañizares P, Rodrigo MA, Linares JJ (2007) *Electrochim Acta* 52:3910
51. He R, Li Q, Xiao G, Bjerrum NJ (2003) *J Memb Sci* 226:169
52. Hasiotis C, Deimede V, Kontoyannis C (2001) *Electrochim Acta* 46:2401
53. Li Q, Pan C, Jensen JO, Noyé P, Bjerrum NJ (2007) *Chem Mater* 19:350
54. Metha V, Cooper JS (2003) *J Power Sources* 114:32
55. Litster S, Mclean G (2004) *J Power Sources* 130:61
56. Lobato J, Rodrigo MA, Linares JJ, Scott K (2006) *J Power Sources* 157:284
57. Seland F, Berning T, Børresen B, Tunold R (2006) *J Power Sources* 160:27
58. Williams J, Krinke A (2005) Fuel cell project. Spring 2005 at <http://faculty.washington.edu/cooperjs/Education/Fuel%20cell%20class/Fuel%20cell%20reports/SP05%20Design%20of%20Experiments.pdf>
59. Duckworth WE (1968) *Statistical techniques in technological research*. Methuen, London
60. Montgomery DC (1976) *Design and analysis of experiments*. Wiley, New York
61. Grujicic M, Chittajallu KM (2004) *Appl Surf Sci* 227:56
62. Chaudhary VA, Mulla IS, Sainkar SR, Mandale AB, Vijayamohan K (2000) *Sens Actuators* 79:224
63. Kannan AM, Shukla AK, Hamnett A (1988) *J Appl Electrochem* 18:149
64. Iwakura Y, Uno K, Imai Y (1964) *J Polym Sci Part A* 2:2605